Suppression of Radixin and Moesin Alters Growth Cone Morphology, Motility, and Process Formation In Primary Cultured Neurons

Gabriela Paglini,* Patricia Kunda,* Santiago Quiroga,‡ Kenneth Kosik,§ and Alfredo Cáceres*

*Instituto Mercedes y Martin Ferreyra-CONICET, 5000 Cordoba, Argentina; ‡Departamento Quimica Biologica (CIQUIBIC), Universidad Nacional Cordoba/CONICET, 5000 Cordoba, Argentina; and §Department of Neurology (Neuroscience), Harvard Medical School, and Center for Neurological Diseases, Department of Medicine, Brigham and Women's Hospital, Boston, Massachusetts 02115

Abstract. In this study we have examined the cellular functions of ERM proteins in developing neurons. The results obtained indicate that there is a high degree of spatial and temporal correlation between the expression and subcellular localization of radixin and moesin with the morphological development of neuritic growth cones. More importantly, we show that double suppression of radixin and moesin, but not of ezrin–radixin or ezrin–moesin, results in reduction of growth cone size, disappearance of radial striations, retraction of the growth cone lamellipodial veil, and disorganization of actin filaments that invade the central region of growth cones where they colocalize with microtubules. Neuritic tips from radixin–moesin suppressed neurons displayed high filopodial protrusive activity; however, its rate of advance is 8–10 times slower than the one of growth cones from control neurons. Radixin–moesin suppressed neurons have short neurites and failed to develop an axon-like neurite, a phenomenon that appears to be directly linked with the alterations in growth cone structure and motility. Taken collectively, our data suggest that by regulating key aspects of growth cone development and maintenance, radixin and moesin modulate neurite formation and the development of neuronal polarity.

Key words: ERM proteins • growth cones • actin filaments • neurite formation • axonal elongation

DEVELOPING neurons often project elongated axons toward their targets over relatively enormous distances. At the distal end of these projections is the growth cone, a highly dynamic structure that contains cytoskeletal elements capable of generating a variety of navigational behaviors that determine the rate and direction of growth, as well as the distribution of membrane receptors that link environmental cues to implementation of specific activities (Bray and Hollenbeck, 1988; Goodman and Shatz, 1993; Tanaka and Sabry, 1995). Lamellipodial veils and filopodial extensions are the most active processes, and are the sites at which growth cones undergo deformations such as elongation and retraction that are fundamental to movement. Currently the detailed molecular assemblies that mediate and regulate growth cone morphology and activity are largely unknown. A crucial aspect for solving this problem is the identification of proteins that mediate interactions between cytoskeletal components and the plasma membrane. In this regard, the highly related ezrin, radixin, and moesin proteins (the ERM[1] proteins) are excellent candidates for molecules playing such a role (Bretscher et al., 1997; Tsukita et al., 1997). These proteins have been localized to cleavage furrows, microvilli, ruffling membranes, and cell–cell/cell–matrix adhesion sites (Bretscher, 1983; Tsukita et al., 1989; Sato et al., 1991; Sato et al., 1992; Berryman et al., 1993) where they appear to play a crucial role in modulating membrane protrusive activity (Takeuchi et al., 1994; Henry et al., 1995; Martin et al., 1995; Martin et al., 1997). In accordance with that, biochemical studies have established that the carboxyl termini of these proteins bind to actin filaments, while the amino terminus interacts with plasma membrane proteins such as CD44 (Tsukita et al., 1994; Hirao et al., 1996; for reviews see Bretscher et al., 1997; Tsukita et al., 1997).

In the particular case of nerve cells, previous studies

Address all correspondence to Alfredo Cáceres, Instituto Mercedes y Martín Ferreyra, Casilla de Correo 389, 5000 Córdoba Argentina. Tel.: 54-51-681465. Fax: 54-51-695163. E-mail: acaceres@immf.uncor.edu

1. *Abbreviations used in this paper*: DIC, differential interference contrast; ERM, ezrin, radixin, and moesin; VEC-DIC, video-enhanced differential interference contrast.

have shown that an mAb designated 13H9 that recognizes an epitope common to all members of the ERM family (Winckler et al., 1994), and a polyclonal antibody against radixin, strongly label growth cone actin-rich structures such as radial striations, lamellipodial veils, and filopodial extensions (Goslin et al., 1989; Birgbauer et al., 1991; DiTella et al., 1994; Gonzalez-Agosti and Solomon, 1996). In addition, functional studies have established that in sympathetic neurons, growth cone collapse induced by NGF deprivation is concomitant with a significant decrease of the radixin staining of growth cones; interestingly, readding NGF, which induces rapid growth cone formation, is accompanied by relocalization of radixin (Gonzalez-Agosti and Solomon, 1996). Besides, the same authors showed that when growth cones were subjected to an electrical field, radixin staining precisely localized to the leading edges in the new direction of growth (Gonzalez-Agosti and Solomon, 1996). Taken collectively, these observations suggest that localization of radixin, and perhaps of ezrin or moesin, may be essential for the normal expression of growth cone morphology and function.

To test this hypothesis directly, we examined the cellular functions of ERM proteins in mammalian neurons. To approach this problem, subcellular fractionation techniques in combination with Western blotting with specific antibodies were used initially to determine which type(s) of ERM proteins are present in growth cones. We then analyzed the pattern of expression, subcellular localization, and consequences of ERM suppression by antisense oligonucleotide treatment on the morphology, cytoskeletal organization, and dynamics of growth cones in primary cultured neurons. The results obtained suggest a key role for radixin and moesin in generating and maintaining the normal structural and functional organization of growth cones.

Materials and Methods

Cell Culture

Dissociated cultures of hippocampal pyramidal cells from embryonic rat brain tissue were prepared as described previously (Cáceres et al., 1986; Mascotti et al., 1997). Cells were plated onto polylysine-coated glass coverslips (12 or 25 mm in diameter) at densities ranging from 5,000 to 15,000 cells per cm^2, and were maintained with DMEM plus 10% horse serum for 1 h. The coverslips with the attached cells were then transferred to 60-mm Petri dishes containing serum-free medium plus the N2 mixture of Bottenstein and Sato (1979). All cultures were maintained in a humidified 37°C incubator with 5% CO_2.

Antisense Oligonucleotides

Two groups of antisense phosphorothioate oligonucleotides (S-modified) were used in this study. The first group consists of antisense oligonucleotides corresponding to positions 1–24 of the mouse ezrin- (As Ez1), radixin- (As Rx1), or moesin- (As Mo1) coding regions, and were identical to those previously used by Takeuchi et al. (1994) to analyze the function of ERM proteins in nonneuronal cells. The second group consists of antisense oligonucleotides corresponding to positions 1387–1404 of the mouse ezrin (As Ez2), 1334–1348 of the mouse radixin (As Rx2), and 1463–1477 of the mouse moesin (As Mo2) coding regions. Analysis of a gene data bank base (Gene Bank) showed that the sequences selected have no significant homology with any other known sequence. The oligonucleotides were purchased from Quality Controlled Biochemicals (Hopkinton, MA); they were purified by reverse chromatography, and were taken up in serum-free medium as described previously (Cáceres and Kosik, 1990; Cáceres et al., 1992; Morfini et al., 1997). For all the experiments the antisense oligonucleotides were preincubated with 2 μl of Lipofectin Reagent (1 mg/ml; GIBCO BRL, Gaithersburg, MD) diluted in 100 μl of serum-free medium. The resulting oligonucleotide suspension was then added to the primary cultured neurons at concentrations ranging from 0.5 to 5 μM. Control cultures were treated with the same concentration of the corresponding sense-strand oligonucleotides or scrambled antisense oligonucleotides.

Primary Antibodies

The following primary antibodies were used in this study: an mAb against tyrosinated α-tubulin (clone TUB-1A2, mouse IgG; Sigma Chemical Co., St. Louis, MO) diluted 1:2,000; a mAb against mouse recombinant ezrin (clone M11, rat IgG, a generous gift of Dr. Sh. Tsukita, Kyoto University, Japan; see also Takeuchi et al., 1994) used undiluted; an mAb against mouse recombinant radixin (clone R21, rat IgG, a generous gift of Dr. Sh. Tsukita, Kyoto University, Japan) used undiluted; an mAb against mouse recombinant moesin (clone M22, rat IgG, a generous gift of Dr. Sh. Tsukita, Kyoto University, Japan; see also Takeuchi et al., 1994) used undiluted; an mAb against human moesin (clone 38, mouse IgG; Transduction Laboratories, Lexington, KY) diluted 1:200; and an affinity-purified rabbit polyclonal antibody raised against a peptide corresponding to amino acids 400–409 (KSAIAKQAAD) of mouse radixin (Research Genetics, Huntsville, AL; see also Winckler et al., 1994) diluted 1:50 or 1:100.

Immunofluorescence

Cells were fixed before or after detergent extraction under microtubule-stabilizing conditions, and were processed for immunofluorescence as previously described (Pigino et al., 1997). For some experiments a mild extraction protocol that preserves cytoskeletal–membrane interactions was also used (Nakata and Hirokawa, 1987; Brandt et al., 1995; Pigino et al., 1997). Cells were washed in extraction buffer (80 mM Pipes, pH 6.8, 1 mM $MgCl_2$, 1 mM EGTA, 30% [vol/vol] glycerol, 1 mM GTP), incubated for 30 s with extraction buffer containing 0.02% saponin, and washed with extraction buffer. Cells were then fixed for 1 h at room temperature with 2% (wt/vol) paraformaldehyde, 0.1% (vol/vol) glutaraldehyde in extraction buffer, washed with PBS, permeabilized with 0.1% (vol/vol) Triton X-100 in PBS for 30 min, and finally washed in PBS. The antibody-staining protocol entailed labeling with the first primary antibody, washing with PBS, staining with labeled secondary antibody (fluorescein- or rhodamine-conjugated) and washing similarly; the same procedure was repeated for the second primary antibody. Incubations with primary antibodies were for 1 or 3 h at room temperature, while incubations with secondary antibodies were performed for 1 h at 37°C. For some experiments, rhodamine-labeled phalloidin (Molecular Probes, Inc.) was included with the secondary antibody to visualize filamentous actin (F-actin). The cells were observed with an inverted microscope (Carl Zeiss Axiovert 35M) equipped with epifluorescence and differential interference contrast (DIC) optics using a 40×, 63×, or a 100× objective (Carl Zeiss). Fluorescent images were captured under regular fluorescence microscopy with a silicon-intensified target camera (SIT-C2400; Hamamatsu Phototonics, Bridgewater, NJ). The images were digitized directly into a Metamorph/Metafluor Image Processor (Universal Imaging Corporation, West Chester, PA). Photographs were printed using Adobe Photoshop.

For some experiments the relative intensities of tubulin, tau, α-actinin, cyclin-dependent kinase 5 (cdk5), β-gc (Mascotti et al., 1997), ezrin, radixin, and moesin immunofluorescence as well as of phalloidin staining were evaluated in fixed unextracted cells or in detergent-extracted cytoskeletons using quantitative fluorescence techniques as described previously (DiTella et al., 1994; DiTella et al., 1996; Pigino et al., 1997). To image-labeled cells, the incoming epifluorescence illumination was attenuated with glass neutral density filters. Images were formed on the faceplate of the SIT camera set for manual sensitivity, gain, and black level; they were digitized directly into the Metamorph/Metafluor Image Processor and stored on laser discs with an optical memory disc recorder (OMDR, LQ-3031, Panasonic). Fluorescence intensity measurements were perfumed pixel by pixel within the cell body and in neurites of identified neurons. Using these data, we then calculated the average fluorescence intensity within the cell body as well as the inner, middle, and distal third of identified neurites (either minor processes or axons), including the central and peripheral regions of growth cones. In addition, in some cases the distribution of phalloidin staining or ERM immunofluorescence were analyzed using high-resolution fluorescence microscopy and ratio image analysis with the image processing menu of the Metamorph/Metafluor system.

Video Microscopy

For time lapse video-enhanced differential interference contrast microscopy (VEC-DIC), hippocampal cells were cultured for up to 3 d in special Petri dishes prepared according to the procedures described by Dotti et al. (1988). At different time points after plating, the dishes containing the attached cells were placed on the heated stage of the inverted microscope and observed with a 100× DIC oil immersion objective. Heat filters and a monochromatic green filter (546 nm) were used to achieve even illumination and reduce damage to cells. DIC images were amplified with a 1.6× relay lens, and were detected with a Newvicon camera (Dage-MTI, Inc., Michigan City, IN). Images were collected every 30 s, summed (32-frame averaging) by using Metamorph software, and stored on a laser disc using the OMDR. Photographs were then printed using Adobe Photoshop.

Subcellular Fractionation Techniques

Fetal rat brain (18 d of gestation) was fractionated according to Pfenninger et al. (1983; see also Quiroga et al., 1995) to obtain growth cone particles (GCPs). In brief, the low-speed supernatant (L) of fetal brain homogenate (H) was loaded on a discontinuous sucrose gradient in which the 0.75 M and 1 M sucrose layers were replaced with a single 0.83 M sucrose step. This procedure facilitated collection of the interface, and increased GCP yield without decreasing purity (Quiroga et al., 1995). The 0.32 M/0.83 M interface, or A fraction, was collected, diluted with 0.32 M sucrose, and pelleted to give the GCP fraction. This was resuspended in 0.32 M sucrose for experimentation.

Western Blot Analysis of ERM Protein Expression

Changes in the levels of ezrin, radixin, and moesin during neuronal development were analyzed by Western blotting as previously described (Morfini et al., 1997; Pigino et al., 1997). In brief, equal amounts of crude brain homogenates, subcellular fractions, or whole cell extracts from cultured cells were separated on SDS-PAGE and transferred to polivinylidene difluoride (PVDF) membranes in a Tris-glycine buffer, 20% methanol. The filters were dried, washed several times with TBS (10 mM Tris, pH 7.5, 150 mM NaCl), and blocked for 1 h in TBS containing 5% BSA. The filters were incubated for 1 h at 37°C with the primary antibodies in TBS containing 5% BSA. The filters were then washed three times (10 min each) in TBS containing 0.05% Tween 20, and were incubated with a secondary horseradish peroxidase–conjugated antibody (Promega Corp., Madison, WI) for 1 h at 37ºC. After five washes with TBS and 0.05% Tween 20, the blots were developed using a chemiluminiscence detection kit (ECL; Amersham Life Science, Inc., Arlington Heights, IL). In addition, ERM protein levels were measured by quantitative immunoblotting as described by Drubin et al. (1985; see also DiTella et al., 1996). For such a purpose, immunoblots were probed with the corresponding primary antibodies, followed by incubation with [^{125}I]protein A. Autoradiography was performed on X-omat AR film (Eastman Kodak Co., Rochester, NY) using intensifying screens. Autoradiographs were aligned with immunoblots, and ERM protein levels were quantitated by scintillation counting of PVDF blot slices.

Morphometric Analysis of Neuronal Shape Parameters

Images were digitized on a video monitor using Metamorph/Metafluor software. To measure neurite length or growth cone shape parameters, fixed unstained or antibody-labeled cells were randomly selected and traced from a video screen using the morphometric menu of the Metamorph as described previously (Cáceres et al., 1992; DiTella et al., 1994; DiTella et al., 1996). All measurements were performed using DIC optics at a final magnification of 768×. Differences among groups were analyzed by the use of ANOVA and Student-Newman Keuls test.

Results

Expression and Subcellular Distribution of ERM Protein in Developing Neurons

Previous studies have shown that antigen 13H9, which corresponds to an epitope common to all members of the

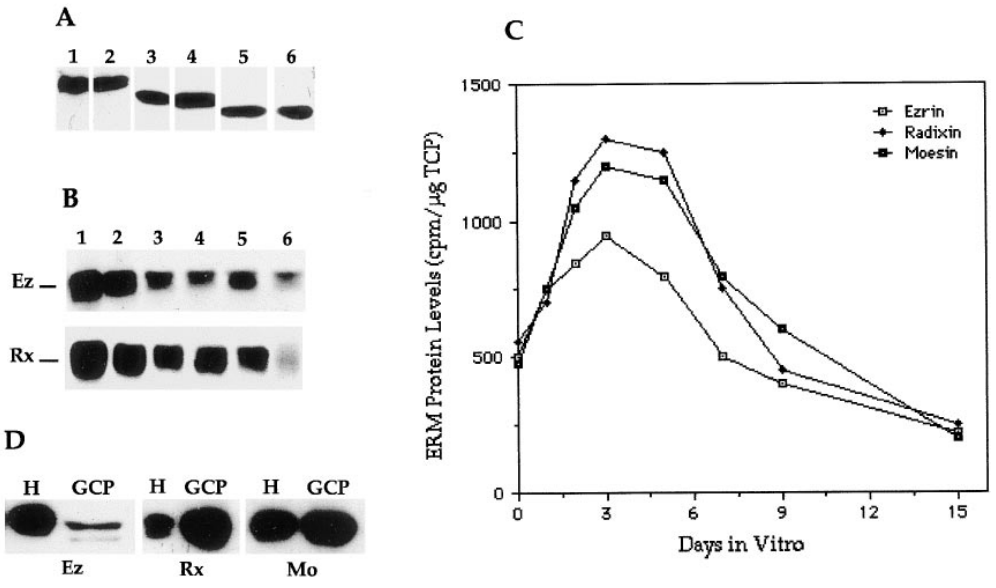

Figure 1. Expression of ERM proteins in developing brain tissue. (*A*) Specificity of the anti-ezrin (mAb M11, lanes *1* and *2*), anti-radixin (affinity-purified peptide antibody; lanes *3* and *4*), and anti-moesin (mAb M22; lanes *5* and *6*) antibodies as revealed by Western blot analysis of whole tissue homogenates obtained from the cerebral cortex of E 18 rat embryos (lanes *1*, *3*, and *5*) or cell extracts from cultured hippocampal pyramidal neurons (lanes *2*, *4*, and *6*). Each of these antibodies labels a single band of 85 kD (anti-ezrin), 82 kD (anti-radixin), or 75 kD (anti-moesin). 10 μg of total protein were loaded in lanes *1*, *3*, *5*, and 30 μg in lanes *2*, *4*, and *6*. (*B*) The expression of ezrin (*Ez*) and radixin (*Rx*) in the developing rat cerebral cortex as revealed by immunoblot analysis of whole tissue extracts. E18 (lane *1*), post-natal day 1 (P1, lane *2*), P3 (lane *3*), P7 (lane *4*), P15 (lane *5*), and P30 (lane *6*). The blots were reacted with the mAb M11 or the affinity-purified rabbit polyclonal antibody against radixin. 40 μg of total protein were loaded in each lane. (*C*) Graph showing the pattern of expression of ERM proteins in cell extracts obtained from cultured hippocampal pyramidal neurons as revealed by quantitative Western blotting (see Materials and Methods). Values are expressed in cpm per μg or total cellular protein (*TCP*). Note that the expression of ERM proteins is high during the first 5 d in vitro, declining gradually but significantly afterwards. (*D*) Western blots showing that ezrin, radixin, and moesin immunoreactive-protein species are present in growth cone particles (*GCP*) isolated by subcellular fractionation. Note the significant enrichment of radixin in the GCP fraction when compared with a total brain homogenate (*H*). 20 μg of protein were loaded in each lane.

ERM family (Winckler et al., 1994), is expressed in cultured hippocampal pyramidal neurons (Goslin et al., 1989), cerebellar macroneurons (DiTella et al., 1994) and dorsal root ganglion neurons (Birgbauer et al., 1991). Despite that, the pattern of expression and subcellular distribution of individual members of the ERM family during neuronal development, both in situ and in vitro, has not yet been established. Therefore, in the first set of experiments we used several antibodies specific for each of these proteins to analyze their expression and subcellular distribution in brain homogenates and cell extracts by Western blotting from developing and adult animals, as well as in growth cone preparations obtained from E 18 rat embryos.

Fig. 1 *A* shows the monospecificity of the mAb M11 against mouse recombinant ezrin, of the affinity-purified rabbit polyclonal antibody raised against a peptide corresponding to amino acids 400–409 (KSAIAKQAAD) of mouse radixin, and of the mAb M22 directed against mouse recombinant moesin. Each of these antibodies labels a single band of 85 kD (anti-ezrin; Fig. 1 *A*, lanes *1* and *2*), 82 kD (anti-radixin; Fig. 1 *A*, lanes *3* and *4*), or 75 kD (anti-moesin; Fig. 1 *A*, lanes *5* and *6*) in Western blots of whole tissue homogenates obtained from the cerebral cortex of E 18 rat embryos, or from cell extracts obtained from cultured hippocampal pyramidal neurons. A commercially available mAb against human moesin (clone 38) also strongly labeled a 75-kD band in embryonic brain extracts, and with a much lower intensity a protein specie migrating at the position of radixin (not shown).

Fig. 1 *B* shows that in the cerebral cortex or hippocampus, expression of the ERM immunoreactive protein species is higher at late embryonic and early postnatal days, declining gradually but significantly until adulthood where the lowest levels are detected; an equivalent expression pattern was detected by quantitative Western blotting of cell extracts obtained from cultures of hippocampal pyramidal neurons (Fig. 1 *C*). In addition, Western blot analysis of GPCs obtained by subcellular fractionation of embryonic brain tissue revealed the presence of each of the ERM members in this compartment (Fig. 1 *D*). This analysis also showed that radixin is the most enriched ERM family member in GPCs, while ezrin is the less abundant.

In the next series of experiments, the subcellular distribution of ERM proteins in cultures of hippocampal pyramidal neurons was analyzed by fluorescence microscopy (Fig. 2). Both undifferentiated and neurite-bearing cells stained with the antibodies against ERM family members; however, significant differences in their staining patterns were detected. Staining with the anti-ezrin antibody (mAb M11) gave intense labeling of cell bodies, while neurites and growth cones stain only very faintly, becoming visible only when the mAb M11 was used at high concentrations. High power views of labeled cells revealed no apparent specific staining of growth cone components (data not shown).

By contrast, radixin and moesin immunofluorescence were not only detected in cell bodies, but also in neurites and growth cones. High-resolution fluorescence microscopy revealed strong radixin staining of the actin-rich peripheral zone of growth cones; within that region, radixin immunolabeling appears to be concentrated at the base of short filopodial extensions that emerge from points all along the growth cone perimeter (Fig. 2, *A–E*). On the other hand, moesin immunofluorescence appears to be concentrated along radial striations that extend from the central growth cone region towards the peripheral lamellipodial veil (Fig. 2, *F–J*) with a pattern that closely resembles the distribution of antigen 13H9 (see also Goslin et al., 1989; DiTella et al., 1994) or F-actin. To test whether localization of radixin or moesin within growth cones involves a plasma membrane association, a mild extraction protocol using saponin was used. This procedure, which selectively removes cytosolic proteins but retains cytoskeletal membrane interactions (Nakata and Hirokawa, 1987; Brandt et al., 1995; see Materials and Methods), did not alter the distribution of either the radixin (Fig. 2, *D* and *E*)

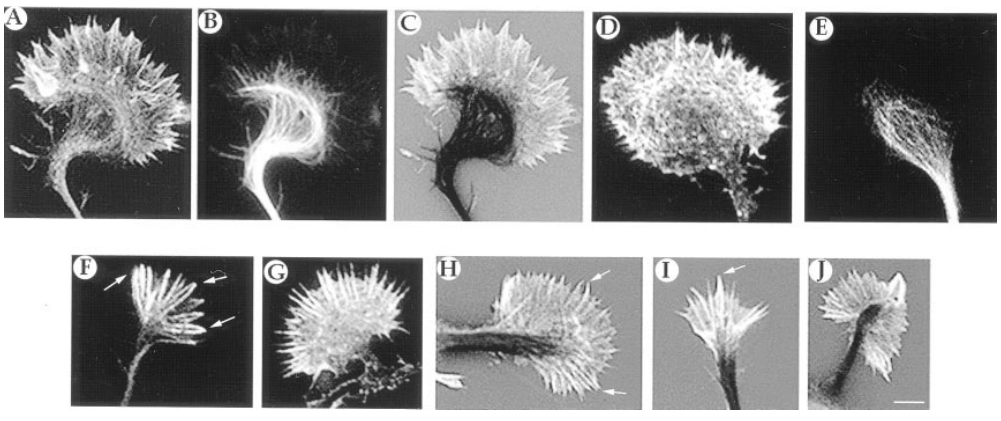

Figure 2. The distribution of radixin and moesin in growth cones. (*A* and *B*) Double immunofluorescence micrographs showing the distribution of radixin (*A*) and tyrosinated α-tubulin (*B*). The images were formed on the faceplate of a SIT camera and digitized directly into the Metamorph/Metafluor Image Processor. Using image *A* as numerator and image *B* as denominator, we applied the ratio image menu of the processor to obtain the image shown in *C* that clearly reveals the presence of radixin immunolabeling in the peripheral lamellipodial veil of the growth cone. (*D* and *E*) Double immunofluorescence micrographs showing another example of the distribution of radixin (*D*) and tyrosinated α-tubulin in axonal growth cones. Note that radixin immunolabeling is highly concentrated at the periphery of growth cones. (*F* and *G*) Immunofluorescence micrographs showing the distribution of moesin (mAb M 22) in growth cones. (*H–J*) Ratio image analysis of the distribution of moesin (*white*) and tubulin (*black*) at neuritic tips. Note that in all cases, moesin immunolabeling is highly concentrated along radial striations extending from the central region of the growth cone towards its periphery (*arrows*). Bar, 5 μm.

or moesin immunolabeling (Fig. 2, *I* and *J*) when compared with that observed in cells fixed before detergent extraction.

Phosphorothioate Antisense Oligonucleotides Inhibit Expression of ERM Family Members

The localization and staining patterns of radixin and moesin are consistent with the possibility that they regulate important features of growth cone formation, maintenance, and/or dynamics. Therefore, to investigate this possibility, we used antisense phosphorothioate oligonucleotides to inhibit expression of ERM proteins. Experimental conditions were optimized as follows. Neurons were cultured for 48 h in serum-free medium, during which time the cells extend three to four minor processes and a single axon; under control conditions all of these neurites are tipped by well-defined growth cones (Cáceres et al., 1986; Cáceres et al., 1992; Mascotti et al., 1997). Antisense, sense, or mismatched oligonucleotides were added to the culture medium 24 h after plating in the presence of Lipofectin, and were replenished every 6 h at concentrations ranging from 0.5 to 2 μM.

Quantitative immunofluorescence analyses indicate that antisense treatment reduced the levels of ERM proteins in a dose- and time-dependent manner (Fig. 3, *A–C*). By 1 d in either 1 or 2 μM of the antisense oligonucleotides specific for individual members of the ERM family, the levels of ezrin, radixin, or moesin had selectively diminished to <20% of the levels within parallel oligonucleotide-free cultures, or from equivalent ones treated with the corresponding sense or mismatched antisense oligonucleotides

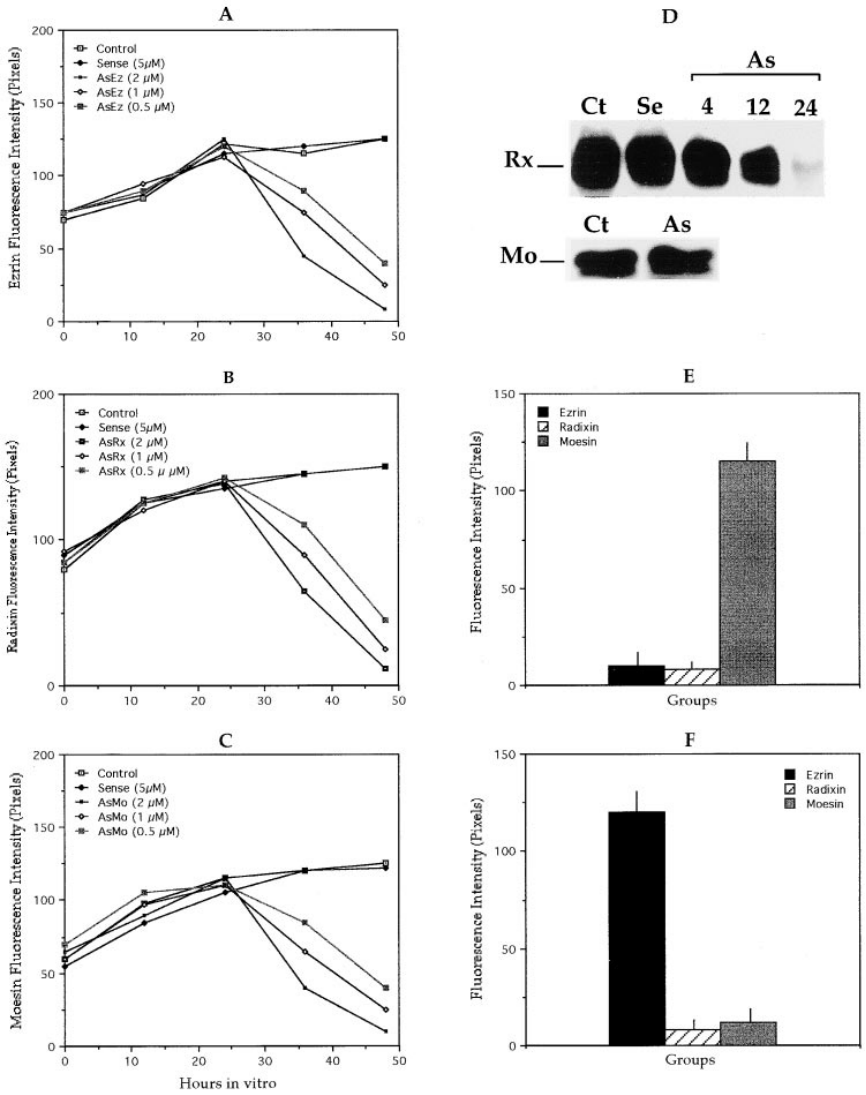

Figure 3. Suppression of ERM protein expression by antisense oligonucleotides. Quantitative analysis of the levels of ERM proteins in hippocampal pyramidal cell cultures treated with antisense, sense, and no oligonucleotides. Protein levels were determined using quantitative immunofluorescence microscopy (*A*, *B*, *C*, *E*, and *F*) or Western blotting (*D*). Measurements of fluorescence intensity (pixels) were performed within the cell body. A total of 100 cells were examined from each condition and time point. Standard deviations were <20 pixels, and error bars were not included because they would be short and blurred together. (*A*) Graph showing the effect of the ezrin antisense oligonucleotide, AsEz (position 1–24 of the mouse ezrin sequence) on ezrin protein levels. (*B* and *C*) Equivalent graphs showing the effect of the radixin (AsRx, position 1–24 of the mouse radixin sequence) or moesin (AsMo, position 1–24 of the mouse moesin sequence) antisense oligonucleotides on radixin and moesin protein levels. Note that the effect of the antisense oligonucleotides are time- and dose-dependent. Sense or antisense oligonucleotides (0.5–5 μM) were added to the culture medium 1 d after plating, and were replenished every 6 h until the end of the experiment. (*D*; *top*) Western blot showing the effect of the radixin antisense oligonucleotide, AsRx2 (2 μM), on radixin protein levels. *Ct*, radixin protein levels in control nontreated cells maintained in culture for 2 d; *Se*, sense-treated cells maintained in culture for 2 d; *As*, radixin protein levels 4, 12, and 24 h after adding the AsRx2 antisense oligonucleotide. (*Bottom*) Western blot showing that the AsRx2 antisense oligonucleotide has no effect on moesin protein levels. *Ct*, moesin protein levels in control nontreated cells maintained in culture for 2 d; *As*, moesin protein levels 24 h after adding the AsRx2 antisense oligonucleotide. Cultures were treated as described previously. (*E* and *F*) Graphs showing the effect of the double suppression of ezrin–radixin (*E*) or radixin–moesin (*F*) on ezrin, radixin, and moesin protein levels. Note that each of the antisense oligonucleotides only decreases the levels of its target protein. For these experiments, antisense oligonucleotides were used at concentrations of 2 μM.

(Fig. 3, *A–C*). By 36 h, ezrin, radixin, or moesin were virtually undetectable in neurons exposed to 1 or 2 μM antisense, and the levels had fallen to <20% of the control levels in neurons exposed to 0.5 μM. Quantitative Western blotting confirmed these observations, and clearly revealed that the antisense oligonucleotides selectively and effectively reduced the levels of individual members of the ERM family (Fig. 3 *D*). Furthermore, adding the ezrin–radixin antisense mixture to the culture medium suppressed both ezrin and radixin expression, but did not affect that of moesin; conversely, the radixin–moesin antisense mixture suppresses both radixin and moesin expression without altering that of ezrin (Fig. 3, *E* and *F*). In this regard, it is worth noting that we could not find any clear cellular compensation for suppressing of one or two ERM family members, as determined by either quantitative fluorescence or Western blotting. In addition, the expression of ERM family members was totally suppressed in the presence of the ezrin–radixin–moesin mixture of antisense oligonucleotides (not shown).

Inhibition of Radixin and Moesin Expression Alters Growth Cone Morphology and Cytoskeletal Organization

In the next series of experiments we analyzed the consequences of ERM suppression on growth cone morphology and cytoskeletal organization. In control or sense-treated neurons, growth cones at the tips of axons consist of a flattened expansion of the cytoplasm of ~10–15 μm across. High-resolution fluorescence microscopy and digital image processing of growth cones from neurons double-stained with antibodies against tyrosinated α-tubulin and rhodamine phalloidin revealed a central microtubule-containing zone completely surrounded by a radially oriented array of F-actin (e.g., actin ribs; see Weinhofer et al., 1997) from which numerous and short filopodial extensions emerge (Fig. 4 *A*). None of the ezrin, moesin, or the pair of ezrin–moesin (Fig. 4 *B*) or ezrin–radixin (Fig. 4 *C*) antisense oligonucleotides induced any significant alteration in growth cone morphology, size, filopodial number, and/or the pattern of distribution of microtubules and actin filaments (Fig. 4, *B* and *C*, and Fig. 5). In sharp contrast, when neurons were cultured in the presence of the radixin–moesin antisense mixture (2 μM), a significant change of growth cone shape was gradually induced. These alterations involved a dramatic reduction of growth cone area, disappearance of radial striations, retraction of the growth cone lamellipodial veil, and a reduction in the number of filopodia; the length of the remaining filopodia increases significantly (Fig. 4, *D–L*; see also Fig. 5). Differences were also detected in the staining pattern of rhodamine–phalloidin. Thus, while in antisense-treated cells, F-actin was concentrated at neuritic tips as in control cells, it was not distributed following specific patterns (e.g., radial striations) but rather had a diffuse appearance filling the entire growth cone, including its central region where it colocalizes extensively with microtubules (Fig. 4, *G–L*). Ratio image analysis of growth cones from cells double-labeled with rhodamine phalloidin and tyrosinated α-tubulin revealed that in neurons lacking radixin and moesin, F-actin predominates over dynamic microtubules within the central region of growth cones (Fig. 4, *G–L*). Thus, a considerable reduction in the number of microtubules entering neuritic tips was evident in cells lacking radixin and moesin; besides, time-course analyses revealed that this phenomenon parallels the reduction of growth cone size observed in these cells. Our results also show that when the medium is changed and replaced by a fresh one lacking the radixin–moesin antisense mixture, the cells reexpress radixin and moesin, a phenomenon paralleled by an increase in growth cone size, the appearance of actin ribs, and lamellipodial veils (Table I).

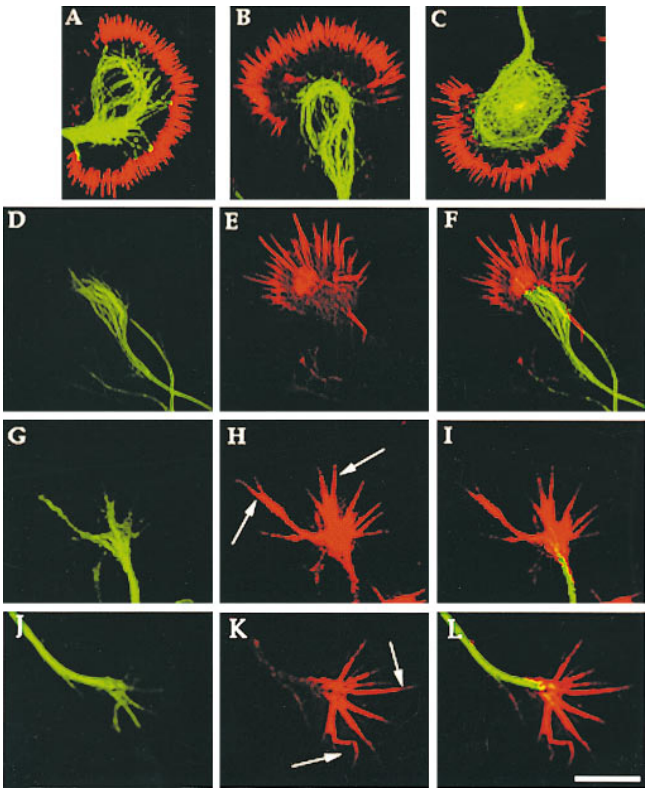

Figure 4. The morphology and cytoskeletal organization of growth cones from control and radixin–moesin suppressed neurons. Red–green overlays of digitized images of growth cones showing the distribution of tyrosinated microtubules (*green*) and F-actin (*red*) in control hippocampal pyramidal neurons (*A*), and in equivalent cells treated with a mixture of ezrin–radixin (*B*) or ezrin–moesin (*C*) antisense oligonucleotides. Images from cells double-stained with an antibody against tyrosinated α-tubulin and rhodamine–phalloidin were formed on the faceplate of a SIT camera and digitized directly into the Metamorph/Metafluor Image Processor; red–green overlays were then generated using Metamorph software. In these growth cones, a central microtubule-containing zone is completely surrounded by a radially oriented array of F-actin. (*D* and *E*) Fluorescence micrographs showing the distribution of tyrosinated α-tubulin (*D*) and rhodamine phalloidin (*E*) in cells treated for 18 h with a mixture of radixin/moesin antisense oligonucleotides (2 μM). (*F*) Red–green overlay of the images shown in *D* and *E*. (*G–L*) Equivalent images to those described previously, but from cells treated with the radixin–moesin antisense mixture for 24 (*G–I*) or 36 (*J–L*) h. Note the progressive alterations in growth cone morphology and in the distribution of F-actin and microtubules. Bar, 10 μm.

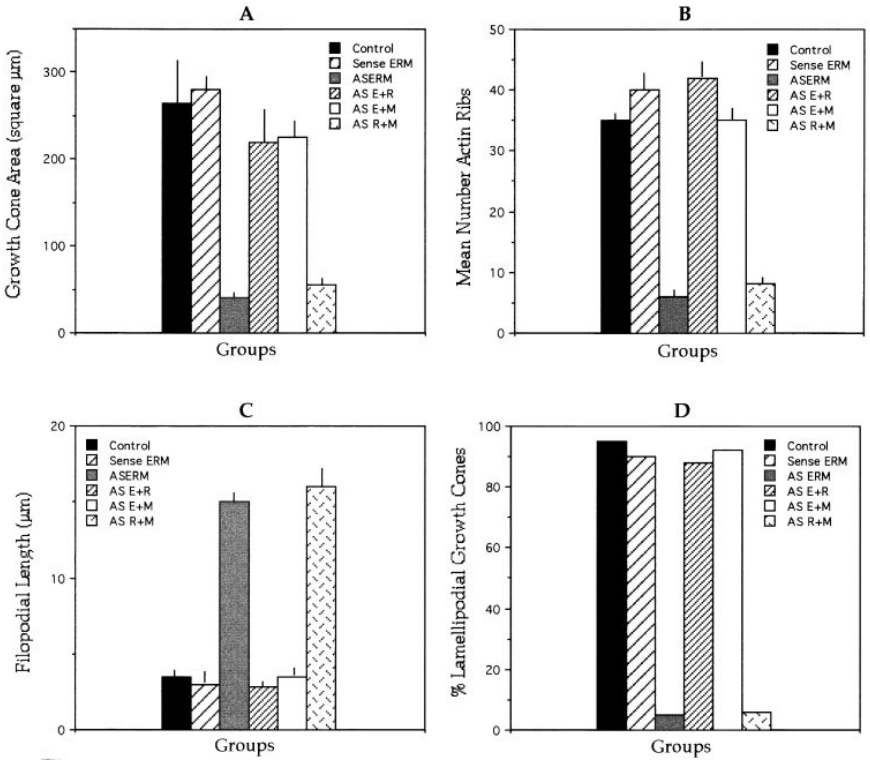

Figure 5. Quantification of growth cone shape parameters in neurons treated with the radixin–moesin antisense mixture. Control, nontreated cells; Sense ERM, cells treated with a mixture of ezrin–radixin–moesin sense oligonucleotides; AS E+R, cells treated with a mixture of ezrin–radixin antisense oligonucleotides; AS E+M, cells treated with a mixture of ezrin–moesin antisense oligonucleotides; AS R+M, cells treated with a mixture of radixin–moesin antisense oligonucleotides. In all cases oligonucleotides were used at a concentration of 2 μM. 200 cells were analyzed for each experimental condition.

Inhibition of Radixin and Moesin Expression Alters Growth Cone Motility

Because of the alterations in growth cone shape and cytoskeletal organization detected in neurons with reduced levels of radixin and moesin, we hypothesized that they may have motility defects. Therefore, we decided to analyze rapid changes in lamellipodial and filopodial activity in control and antisense-treated neurons using time-lapse VEC-DIC microscopy. As expected, according to previous observations from this and other laboratories (see Goldberg and Burmeister, 1986; Kleitman and Johnson, 1989; Lu et al., 1997), in control and sense-treated neurons, axons gradually elongate by cycles of lamellipodial protrusions and retractions, engorgement of the central domain of the growth cone, and consolidation of the neurite. In these cells the leading margins of lamellipodia advance slowly and smoothly across the substratum at a rate of 0.08–0.15 μm/min (Fig. 6). Time-lapse sequences revealed that after the leading edge of a lamellipodial veil have advanced 6–8 μm, a new axonal segment of ~4–6 μm in length is formed at the base of the growth cone. A completely different picture was observed in neurons treated with the radixin–moesin antisense oligonucleotide mixture; in these cells axonal tips, which lack a lamellipodial veil, advance 8–10 times slower than control growth cones; this phenomenon is paralleled by a dramatic inhibition in the rate of axonal elongation (Fig. 6).

On the other hand, they display high filopodial protrusive activity (Fig. 7). This increased activity may be due to a delayed retraction of filopodia and/or an enhanced rate of filopodial extension. To test for these possibilities, sequences from control, sense-treated, and antisense-treated cultures were analyzed for the duration of filopodial persistence or the rate of filopodial elongation. In nontreated (Fig. 7, *A–C*), sense-treated (Fig. 7, *D–F*), or in cells treated with a mixture of ezrin–radixin or ezrin–moesin antisense oligonucleotides (not shown), 75% of filopodia

Table I. The Inhibitory Effects of the Radixin–antisense Oligonucleotides Are Reversible

	Hours after release from antisense treatment		
Antisense treatment	0	12	24
Nontreated			
Radixin fluorescence intensity	125 ± 10	128 ± 8	132 ± 8
Moesin fluorescence intensity	106 ± 4	110 ± 6	110 ± 4
Growth cone area	255 ± 35		240 ± 28
Mean number actin ribs	35 ± 5		38 ± 6
Radixin–moesin sense-treated			
Radixin fluorescence intensity	128 ± 12		126 ± 12
Moesin fluorescence intensity	108 ± 10		108 ± 10
Growth cone area	240 ± 20		265 ± 15
Mean number actin ribs	38 ± 6		44 ± 8
Radixin–moesin antisense-treated			
Radixin fluorescence intensity	6 ± 0.5	44 ± 12	85 ± 10
Moesin fluorescence intensity	8 ± 0.9	38 ± 10	78 ± 12
Growth cone area	45 ± 5	86 ± 10	187 ± 14
Mean number actin ribs	8 ± 2	14 ± 4	26 ± 6

Cultures were treated with the radixin–moesin sense or antisense oligonucleotide mixture (2 μM) for 24 h; after that time the medium was replaced with a fresh one lacking oligonucleotides, and the cells were analyzed at different time intervals after the release of the treatment. Data are expressed as the mean ± SEM. Radixin and moesin levels were determined by quantitative fluorescence as described in the Materials and Methods section. Measurements were performed within the cell body, and are expressed in pixels. Area values are expressed in μm^2. 100 cells were analyzed for each time point and experimental condition.

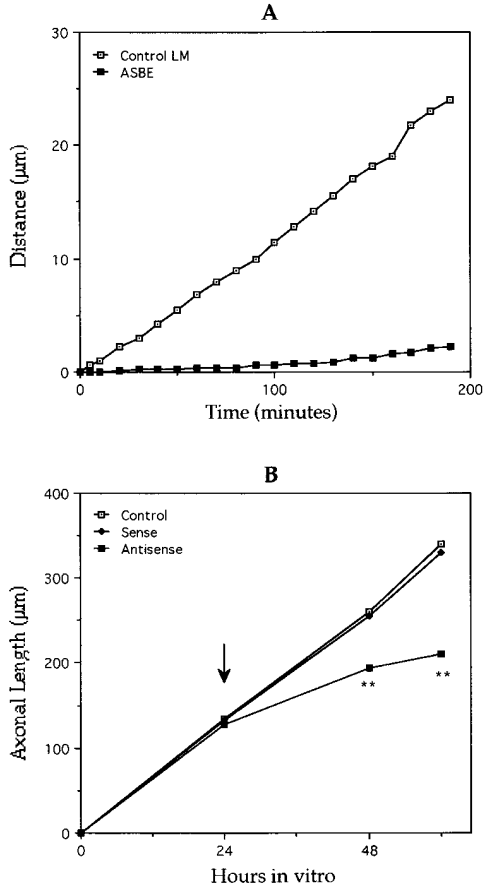

Figure 6. (*A*) Graph showing the rate of advance of the leading edge of lamellipodial growth cones from control nontreated cells (*Control LM*) and from axonal tips (*BE*, blunt ends) of cells treated with a mixture of radixin–moesin antisense oligonucleotides (*ASBE*). Time-lapse sequences were obtained from cells maintained in culture for 2 d; the antisense oligonucleotide mixture (2 μM) was added to the culture medium 1 d after plating, and was replenished every 6 h until the end of the experiment. 50 cells were analyzed for each experimental condition. Standard deviations were <5 μm; 50 cells were analyzed for each experimental condition. (*B*) Graph showing changes in axonal length in control (nontreated), sense-, and antisense-treated hippocampal pyramidal neurons. Radixin–moesin oligonucleotides (sense or antisense) were added to the tissue culture medium 1 d after plating (*arrow*) at a concentration of 2.5 μM. 250 cells were analyzed for an experimental condition at each time point. Standard deviations were <20 μm, and error bars were not included because they would be short and blurred together. *Values significantly different from those of control or sense-treated neurons.

lasted 1 min or less. The curve of filopodial persistence declined steeply: 85% lasted <3 min, and none lasted >10 min. In sharp contrast, more than 90% of growth cone filopodia from cells with the double suppression of radixin and moesin lasted for more than 20 min, with 55% failing to retract after 30 min (Fig. 7, *G–L*). The life histories of individual filopodia from control and antisense-treated neurons were studied frame by frame. These histories demonstrate that in control cells, filopodia went to elongation/pause phases and/or rapid linear retraction phases. Antisense-treated neurons also exhibited similar phases. However, during the elongation phase, the rate of elongation of cells treated with the radixin–moesin antisense mixture was 0.45 ± 0.08 μm/min (n = 100), which was significantly higher ($P < 0.01$) than that of nontreated cells (0.12 ± 0.02 μm/min, n = 50), radixin–moesin sense-treated (0.15 ± 0.04, n = 50) cells, or cells treated with an ezrin–radixin antisense mixture (0.13 ± 0.03, n = 40). Even more dramatic differences were observed when we analyzed the retraction phase. Thus, the rate of retraction was more than threefold slower in the radixin–moesin antisense-treated neurons than in control ones (Fig. 8 *A*). Furthermore, the dynamic pattern of filopodial retraction was also different. Thus, in control cells most of the filopodia retracted in an all-or-none fashion (see Lu et al., 1997); that is, once retraction began it continued until completion. Only a small percentage (<10%) retracted in a discontinuous fashion, in which retraction was interrupted by either a pause phase or an elongation/pause phase. On the other hand, >90% of the radixin–moesin antisense-treated cells exhibit this behavior, with <5% accounting for the all-or-none retraction pattern. This analysis revealed that during the retraction phase, filopodia from radixin–moesin-suppressed neurons tended to pause for significantly longer time periods than did filopodia from control neurons (Fig. 8 *B*).

Development of Neuronal Polarity in Radixin–Moesin-suppressed Neurons

The dramatic alterations in growth cone organization and motility observed in neurons lacking radixin and moesin raised the possibility of these cells having significant alterations in process formation. Therefore, we decided to examine the consequences of radixin and moesin suppression on neurite outgrowth and development of neuronal polarity. For such a purpose, cells were treated with the antisense oligonucleotides shortly after plating, when most of the cells lack neurites, and were examined 24 and 36 h later. The results obtained indicate that neither the single suppression of ezrin, radixin, or moesin, nor the double suppression of ezrin and radixin or ezrin and moesin alters the neurite outgrowth response of these cells when compared with the one observed in control or sense-treated cultures (Table II). Besides, in all cases these neurons follow a predictable temporal sequence of gross morphological changes that involves initial extension of a lamellipodial veil (Stage I) that is later replaced by three to four minor neurites (Stage II), one of which becomes the neuron's axon (Stage III).

On the other hand, the mixture of radixin–moesin antisense oligonucleotides profoundly affects development of these neurons in a dose-dependent manner (Table II and Fig. 9). The most significant alterations, which were observed when the neurons were treated with 2 μM of the antisense mixture, involved: (*a*) a decrease in the length of minor processes and in the percentage of cells reaching stage III of neuritic development; (*b*) a reduction in growth cone area; and (*c*) the appearance of long filopodial extensions emerging from the cell bodies and neuritic tips (see Fig. 9, *G–H*). No such alterations were observed when the cells were treated with a mixture of the corresponding sense oligonucleotides (Table II).

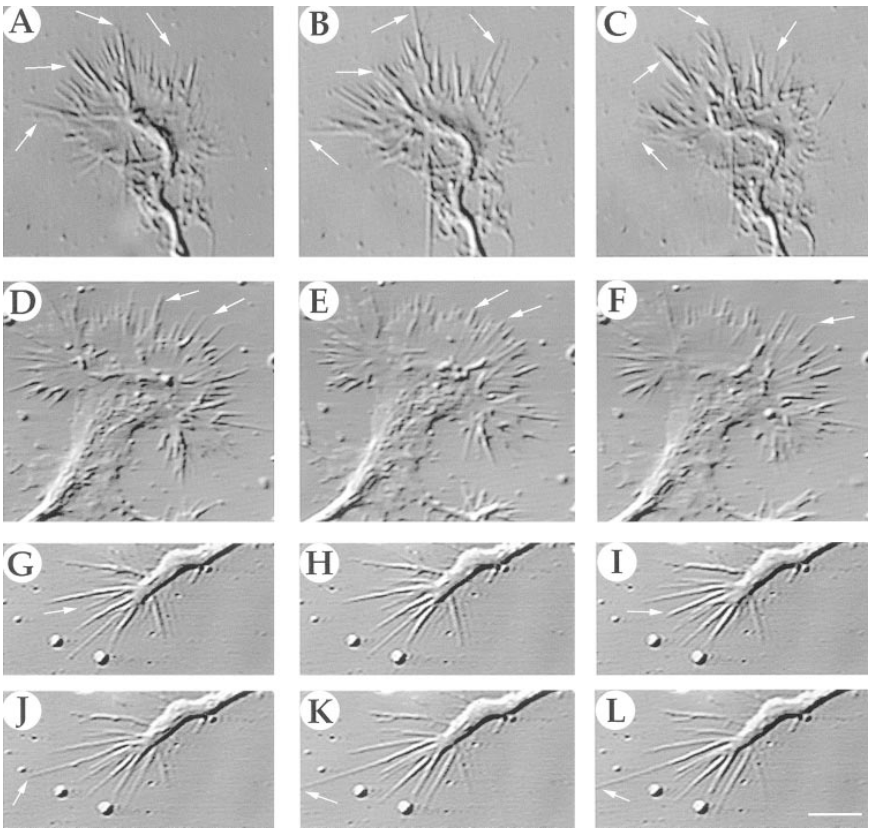

Figure 7. Suppression of radixin and moesin alters filopodial protrusive activity. (*A–C*) A sequence of VEC-DIC images of an axonal growth cone from a control hippocampal cell culture The images were recorded at 2 d in culture. The total length of the sequence shown is 4 min, and each image was taken at 2-min intervals. (*D–F*) An equivalent sequence to that shown previously but from a culture treated with a mixture of radixin–moesin sense oligonucleotides. (*G–I*) A sequence of VEC-DIC images of an axonal growth cone from an hippocampal cell culture treated for 24 h with a mixture of radixin–moesin antisense oligonucleotides (position 1–24 of the radixin and moesin sequences) used at a concentration of 2 μM. The images were also recorded 2 d after plating; they were taken at 0.5 (*G*), 2 (*H*), 4 (*I*), 18 (*J*), 20 (*K*), and 22 (*L*) min after the beginning of the recording. Note that the axonal tip lacks a lamellipodial veil as opposed to control growth cones. Note also that most of the filopodia failed to retract, and some of them elongate considerably (*arrows*). Bar, 5 μm.

It has recently been shown that in cultured hippocampal pyramidal neurons, it is possible to identify the prospective axon by the appearance of a large growth cone in one of the multiple minor processes (Bradke and Dotti, 1997; see also Morfini et al., 1994). Since the radixin–moesin antisense mixture significantly decreases the number of cells entering stage III, it became of interest to determine whether or not growth cone enlargement occurs in stage II hippocampal pyramidal neurons treated with the radixin–moesin antisense oligonucleotide mixture. To address this issue, growth cone surface area was measured in the neurites of stage II cells from control and antisense-treated neurons. Frequency histogram analyses of growth cone area revealed that in nontreated or sense-treated cultures, more than 50% of stage II cells exhibit a single growth cone that was significantly larger than the others (Figs. 9 and 10). By contrast, none of stage II cells from cultures treated with the radixin–moesin antisense mixture display this pattern; most of the cells have small growth cones of uniform size.

Discussion

In nonneuronal cells, ERM proteins play crucial structural and regulatory roles by stabilizing specialized plasma membrane domains such as microvilli and membrane ruffles (see Bretscher et al., 1997; Tsukita et al., 1997). The present observations are fully consistent with this idea, and provide the first set of direct experimental evidence revealing the functional involvement of ERM family members in neuronal morphogenesis. Several lines of evidence support this proposal. First, we found a high degree of spatial and temporal correlation between the expression and subcellular localization of radixin and moesin with the morphological development of neuritic growth cones. Second, and perhaps more importantly, double suppression of these proteins with a mixture of antisense oligonucleotides results in dramatic alterations of growth cone shape, distribution of actin filaments, and locomotive activity of growth cones. The fact that we observed growth cone alterations only after double suppression of radixin and moesin, but not after ezrin–radixin or ezrin–moesin suppression, is not unexpected. Treating nonneuronal cells with mixtures of antisense oligonucleotides against ERM family members has revealed that these proteins can be functionally substituted (Takeuchi et al., 1994). However, this redundancy appears to be cell type–specific. Thus, in thymoma and mouse epithelial cells, ezrin and radixin, rather than the combination of radixin–moesin, appear to have redundant functions, while moesin has some synergetic functional interaction with the two other family members (Takeuchi et al., 1994). On the other hand, in 3T3 fibroblasts, displacement of moesin by exogenously expressed radixin occurs without any apparent phenotype such as alterations in spreading or cytokinesis, suggesting that in these cells radixin and moesin can be functionally substituted (Henry et al., 1995). Differences in the use of ERM family members among different cell types may reflect the very distinct and restricted patterns of expression of these proteins in cell tissues, and/or variations in their subcellular distribution (Amieva et al., 1994; Amieva and Furthmayr, 1995; Berryman et al., 1993; Takeuchi et al.,

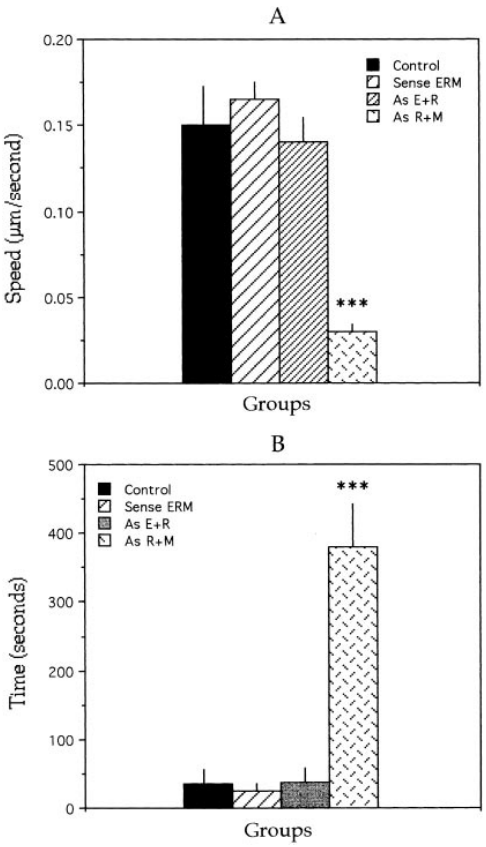

Figure 8. (*A*) Graph showing that the rate of retraction of filopodia during the retraction phase is significantly slower (*$P <$ 0.001) in cells treated with the radixin–moesin antisense mixture (As R+M) than in control cells, or than in cells treated with a mixture of ezrin–radixin–moesin sense oligonucleotides (Sense ERM) or with a mixture of ezrin–radixin antisense oligonucleotides (As E+R). (*B*) Graph showing that the pause/elongation phase during retraction of filopodia was significantly longer (*$P <$ 0.001) in cells treated with the radixin–moesin antisense mixture than in the other groups. For all these experiments oligonucleotides were used at a concentration of 2 μM.

1994; Schwartz-Albiez et al., 1995; Bretscher et al., 1997). In agreement with that, we showed by quantitative immunofluorescence of cultured neurons and Western blotting of growth cone fractions that only radixin and moesin are concentrated in growth cones; ezrin was mainly restricted to the cell body.

Table II. Suppression of Radixin–moesin Inhibits Process Formation in Cultured Hipocampal Pyramidal Cells

Treatment	Minor processes	Stage II	Stage III
	total length/neuron	%	%
Nontreated	55 ± 5	55 ± 4	35 ± 6
Sense-treated	65 ± 8	56 ± 5	33 ± 8
Ezrin–radixin antisense-treated	50 ± 8	52 ± 8	30 ± 5
Radixin–moesin antisense-treated	24 ± 4	88 ± 6	4 ± 0.5

Cultures were treated with the radixin–moesin sense or antisense oligonucleotide mixture (2 μM) for 24 h from the time of plating. Data are expressed as the mean ± SEM. Length values are expressed in μm. Stage II cells were those with a symmetric array of short neurites of equivalent length; Stage III cells were those with a neurite that exceeds others from the same cells by >25 μm in length (Dotti et al., 1988; Cáceres et al., 1992). 100 cells were analyzed for each time point and experimental condition.

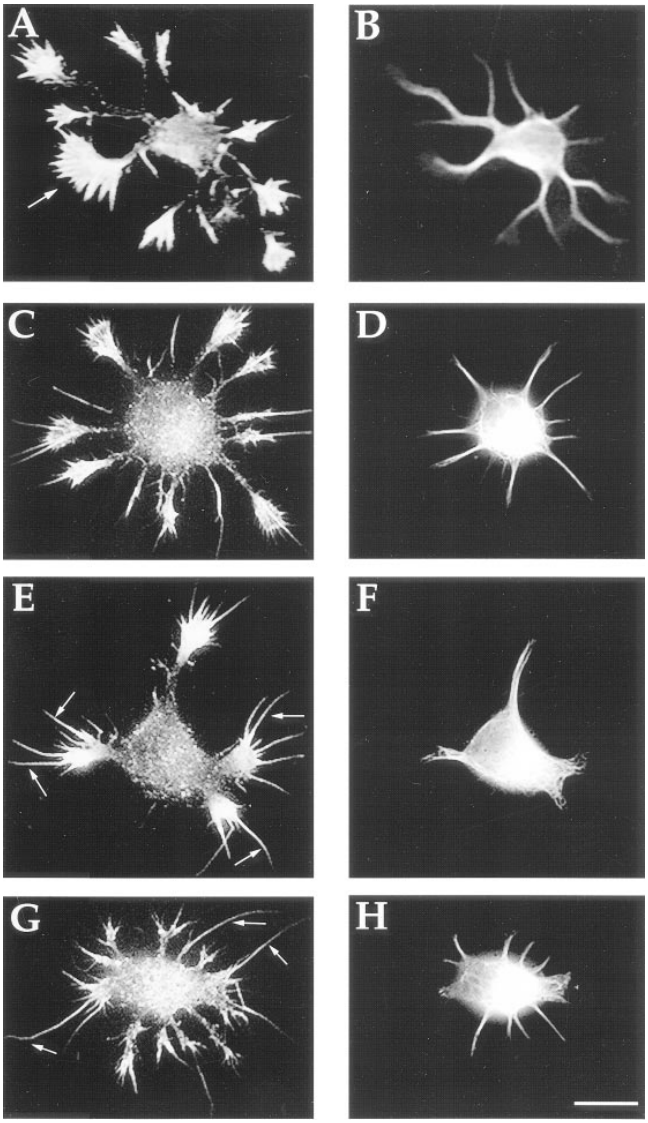

Figure 9. Suppression of radixin and moesin inhibits neurite outgrowth. Fluorescence micrographs showing examples of stage II hippocampal pyramidal neurons from control nontreated (*A* and *B*) or antisense-treated cultures (*C–H*). The oligonucleotides were added 2 h after plating, and were replenished every 6 h until the end of the experiment. They were used at concentrations of 0.5 (*C–D*), 1 (*E–F*), and 2 (*G–H*) μM. All cultures were fixed 1 d after plating. The cells were stained with rhodamine–phalloidin, and with an antibody against tyrosinated α-tubulin. Note the progressive alterations in growth cone morphology, the appearance of long filopodial extensions (*arrows*), and the short length of neuritic shafts in the antisense-treated neurons. Also note that while control neurons exhibit a growth cone that is significantly larger (*A*, *arrow*) than the other ones from the same cell, none of the stage II cells from cultures treated with the radixin–moesin antisense mixture display this pattern. Neurons treated with a mixture of radixin–moesin sense oligonucleotides are indistinguishable from control nontreated ones (not shown). Bar, 10 μm.

Recent observations of living growth cones using Helisoma neurons as a model system have established that

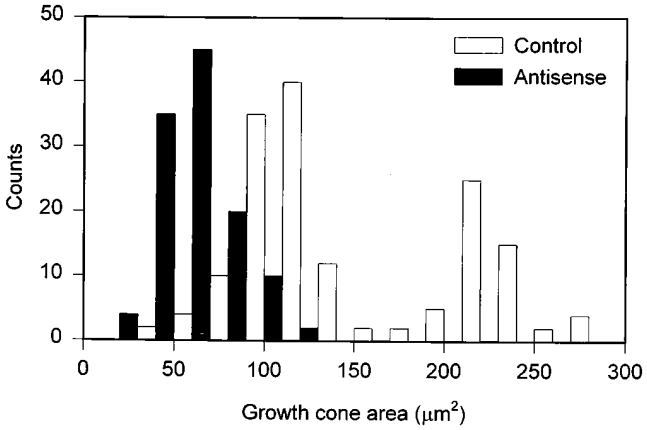

Figure 10. Frequency histogram analysis of growth cone area in control nontreated stage II hippocampal pyramidal neurons, and in equivalent cells but from cultures treated with a mixture of radixin–moesin antisense oligonucleotides (2 μM). Note that while in control neurons there are two populations of growth cones, in the antisense-treated neurons there is only one population of reduced size.

growth cone formation is characterized by a three-stage process involving sequential appearance of a terminal swelling, extension of radial striations—a chevron arrangement of actin ribs—and formation of a lamellipodial veil. After a continuous lamellipodium has surrounded the terminal swelling, growth cones continue to increase in size as a result of lateral and centrifugal extensions (Welnhofer et al., 1997). Since disappearance of radial striations and lamellipodial veils and reduction of growth cone size are early and typical features of neuritic tips from neurons lacking radixin–moesin, it follows that these proteins appear to regulate key stages of growth cone morphogenesis. Such a role is fully consistent with current views about the involvement of ERM family members in regulating cortical structures. Administration of antisense oligonucleotides to suppress ERM protein expression results in loss of cell surface microvilli and cell contacts (Takeuchi et al., 1994). On the other hand, overexpression of the COOH-terminal domains of ezrin or radixin, which may sequester a substantial portion of F-actin and associated proteins, results in dramatic reorganization of the cortical cytoskeleton (Henry et al., 1995; Martin et al., 1995; Martin et al., 1997) while overexpression of the NH_2-terminal domain, acting as a negative dominant mutant by inactivating COOH-terminal domains, reduces microvilli formation (Crepaldi et al., 1997). On the basis of these and related observations, it has been proposed that ERM family members working in conjunction with actin cross-linkers may promote assembly of actin-rich surface structures by linking the sides of actin filaments to plasma membrane proteins (Tsukita et al., 1989; Roy et al., 1997; Bretscher et al., 1997; Tsukita et al., 1997). In support of this we found that in neurons expressing reduced levels of radixin and moesin, growth cone alterations were paralleled by a dramatic disorganization of F-actin.

Inhibition of radixin and moesin expression also result in the appearance of several long filopodial processes at the tip of neurites; these structures appear to arise by impaired retraction and increased filopodial extrusion. While the reason(s) for this phenotype are not clear, at present several possibilities should be considered. For example, long filopodial extensions may arise if ERM proteins also contribute to the regulation of actin assembly by capping actin filament ends at restricted sites (Mitchison and Kirschner, 1988; Forscher et al., 1992). In this regard it is worth noting that radixin was originally isolated as a barbed-end capping protein (Tsukita et al., 1989), and that recent studies suggest that the nature of the interaction of ERM family members with actin may be far more complex than originally expected (Berryman et al., 1995; Bretscher et al., 1997). Alternatively, these long filopodial processes may not simply represent the consequences of suppressing radixin and moesin, but rather arise as a result of an imbalance in the activity of other actin-associated proteins involved in regulating length changes of filopodia, such as myosin-V (Lin et al., 1996). Clearly, additional studies are required for distinguishing between these and related possibilities.

Analysis of the phenotype of neurons expressing low levels of radixin and moesin also revealed an inhibition of their neurite outgrowth response. It is likely that this negative response is directly linked with alterations in growth cone structure and motility. In fact, there is a considerable body of evidence indicating that growth cone formation is essential for proper neurite extension and differentiation (Goldberg and Burmeister, 1986; Weinhofer et al., 1997). Besides, according to current models, the cycle of lamellipodial protrusion, extension, and adhesion to the substrate will promote generation of tension to move the growth cone and its content (Joshi et al., 1985; Mitchison and Kirschner, 1988; Letourneau, 1997). In support of this finding, it has been shown that fully developed lamellipodial growth cones translocate several times faster than either neuritic tips containing only filopodial extensions or blunt ends (Kleitman and Johnson, 1987). The disappearance of radial striations and lamellipodial veils may therefore significantly affect process extension by reducing the surface membrane at the leading edge, and hence decreasing the force generation capability of growth cones. Additional events may also account for the reduced rate of elongation. For example, since growth cones are the preferred sites for adding newly synthesized membrane proteins during elongation (Pfenninger and Mayle-Pfenninger, 1981; Lockerbie et al., 1991; Craig et al., 1995; Bradke and Dotti, 1997), preventing advance of microtubules not only into the peripheral domain of the leading edge, but also into its central domain, may affect process extension by decreasing the membrane vesicle content of neuritic tips. In favor of this view, we found that actin disorganization was accompanied by a significant decrease in the number of microtubules entering the growth cones and in the bodipy–ceramide staining of neuritic tips (Cáceres and Paglini, unpublished observations); besides, time-lapse video microscopy revealed no evidence of engorgement of these neuritic tips.

In cultured hippocampal pyramidal neurons, neuronal polarization occurs at the transition between stages II and III, when one of the multiple minor neurites initiates a phase of rapid elongation to become the neuron's axon

(Dotti et al., 1988). It has recently been shown that one of the earliest events preceding axonal formation is the appearance of a large growth cone in one of the minor neurites (Bradke and Dotti, 1997). No such increase in growth cone size was detected in stage II cells from cultures treated with the mixture of radixin–moesin antisense oligonucleotides. All growth cones display reduced size, and lack radial striations and lamellipodial veils. Besides, the percentage of cells reaching stage III of neuritic development was dramatically reduced. These phenotypes are not simply the consequence of suppressing any growth cone actin-regulatory protein, since for example, hippocampal pyramidal neurons from gelsolin-null mice that display delayed filopodial retraction extend axons and elongate neurites at a rate similar to that of their counterparts in wild-type animals (Lu et al., 1997). Therefore, our results also suggest that radixin and moesin modulate the development of neuronal polarity by regulating key aspects of growth cone development and maintenance.

The authors express their deep gratitude to Dr. Sh. Tsukita (Kyoto University, Japan) for providing some of the antibodies used in this study.

This work was supported by grants from CONICET (PICT-PIP 0052), CONICOR, Fundación Perez-Companc, Fundación Antorchas, and a Fogarty International Collaborative Award (FIRCA). It was also supported by a Howard Hughes Medical Institute grant to A. Cáceres (HMMI 75197–553201) awarded under the International Research Scholars Program. G. Paglini and P. Kunda are fellows from the National Council of Research from Argentina (CONICET).

Received for publication 30 April 1998 and in revised form 10 September 1998.

References

Amieva, M., O. Turumen, A. Vaheri, D. Louvard, and M. Arpin. 1994. Radixin is a component of hepatocyte microvilli in situ. *Exp. Cell Res.* 210:140–144.

Amieva, M., and H. Furthmayr. 1995. Subcellular localization of moesin in dynamic filopodia, retraction fibers, and other structures involved in substrate exploration, attachment, and cell-cell contacts. *Exp. Cell Res.* 219:180–196.

Berryman, M., Z. Frank, and A. Bretscher. 1993. Ezrin is concentrated in the apical microvilli of a wide variety of epithelial cells, whereas moesin is found primarily in endothelial cells. *J. Cell Sci.* 105:1025–1043.

Berryman, M., R. Gary, and A. Brestcher. 1995. Ezrin oligomers are major cytoskeletal components of placental microvilli: a proposal for their involvement in cortical morphogenesis. *J. Cell Biol.* 131:1231–1241.

Birgbauer, E., J. Dinsmore, B. Winckler, A. Lander, and F. Solomon. 1991. Association of ezrin isoforms with the neuronal cytoskeleton. *J. Neurosci. Res.* 30:232–241.

Bottenstein, J., and G. Sato. 1979. Growth of a rat neuroblastoma cell line in a serum-free supplemented medium. *Proc. Natl. Acad. Sci. USA.* 81:5613–5617.

Bradke, F., and C. Dotti. 1997. Neuronal polarity: vectorial cytoplasmic flow precedes axonal formation. *Neuron.* 19:1175–1186.

Brandt, R., J. Leger, and G. Lee. 1995. Interaction of tau with the neural plasma membrane mediated by tau's amino-terminal projection domain. *J. Cell Biol.* 131:1327–1340.

Bray, D., and P. Hollenbeck. 1988. Growth cone motility and guidance. *Annu. Rev. Cell Biol.* 4:43–61.

Bretscher, A. 1983. Purification of a 80000-dalton protein that is a component of the isolated microvilli cytoskeleton, and its localization in nonmuscle cells. *J. Cell Biol.* 108:921–930.

Bretscher, A., D. Reczek, and M. Berryman. 1997. Ezrin: a protein requiring conformational activation to link microfilaments to the plasma membrane in the assembly of cell surface structures. *J. Cell Sci.* 110:3011–3018.

Cáceres, A., G. Banker, and L. Binder. 1986. Immunocytochemical localization of tubulin and microtubule-associated protein 2 during the development of hippocampal neurons in culture. *J. Neurosci.* 6:714–722.

Cáceres, A., and K.S. Kosik. 1990. Inhibition of neurite polarity by antisense oligonucleotides in primary cerebellar neurons. *Nature.* 343:461–463.

Cáceres, A., J. Mautino, and K.S. Kosik. 1992. Suppression of MAP2 in cultured cerebellar macroneurons inhibits minor neurite formation. *Neuron.* 9:607–618.

Craig, A., R. Wyborski, and G. Banker. 1995. Preferential addition of newly synthesized membrane proteins at axonal growth cones. *Nature..* 375:592–594.

Crepaldi, T., A. Gautreau, P. Connoglio, D. Louvard, and M. Arpin. 1997. Ezrin is an effector of hepatocyte growth factor-mediated migration and morphogenesis in epithelial cells. *J. Cell Biol.* 138:423–434.

DíTella, M., F. Feiguin, G. Morfini, and A. Cáceres. 1994. Microfilament-associated growth cone component depends upon tau for its intracellular localization. *Cell Motil. Cytoskelet.* 29:117–130.

DiTella, M., F. Feiguin, G. Morfini, and A. Cáceres. 1996. MAP1b/tau functional redundancy during laminin-enhanced axonal growth. *J. Cell Sci.* 109: 467–477.

Dotti, C., C. Sullivan, and G. Banker. 1988. The establishment of polarity by hippocampal neurons in culture. *J. Neurosci.* 8:1454–1468.

Drubin, D., S. Feinstein, E. Shooter, and M. Kirschner. 1985. Nerve growth factor-induced neurite outgrowth in PC12 cells involves the coordinate induction of microtubule assembly and assembly promoting factors. *J. Cell Biol.* 101:1799–1807.

Forscher, P., C. Lin, and C. Thompson. 1992. Novel from of growth cone motility involving site-directed actin filament assembly. *Nature..* 357:515–518.

Goldberg, D., and D. Burmeister. 1986. Stages in axon formation: observations of growth of Aplisia axons in culture using video-enhanced contrast differential interference microscopy. *J. Cell Biol.* 103:1921–1931.

Gonzalez-Agosti, C., and F. Solomon. 1996. Response of radixin to perturbations of growth cone morphology and motility in chick sympathetic neurons in vitro. *Cell Motil. Cytoskelet.* 34:122–136.

Goodman, C., and C. Shatz. 1993. Developmental mechanisms that generate precise patterns of neuronal connectivity. *Cell.* 72(Suppl.):77–98.

Goslin, K., E. Birgbauer, G. Banker, and F. Solomon. 1989. The role of the cytoskeleton in organizing growth cones: A microfilament-associated growth cone component depends upon microtubules for its localization. *J. Cell Biol.* 109:1621–1631.

Joshi, H., D. Chu, E. Buxbaum, and S. Heidemann. 1985. Tension and compression in the cytoskeleton of PC12 neurites. *J. Cell Biol.* 101:697–705.

Henry, M., C. Gonzalez-Agosti, and F. Solomon. 1995. Molecular dissection of radixin: distinct and interdependent function of the amino- and carboxy-terminal domains. *J. Cell Biol.* 129:1007–1022.

Hirao, M., N. Sato, T. Kondo, S. Yonemura, M. Monden, T. Sasaki, Y. Takai, Sh. Tsukita, and Sa. Tsukita. 1996. Regulation mechanism of ERM protein/plasma membrane association: possible involvement of phosphatidylinositol turnover and Rho-dependent signaling pathway. *J. Cell Biol.* 135:37–51.

Kleitman, N., and M. Johnson. 1987. Rapid growth cone translocations on laminin is supported by lamellipodial not filopodial structures. *Cell Motil. Cytoskelet.* 13:288–300.

Letourneau, P. 1997. The cytoskeleton in nerve growth cone motility and axonal pathfinding. *Perspect. Dev. Neurobiol.* 4:111–123.

Lin, C., E. Espreafico, M. Mooseker, and P. Forscher. 1996. Myosin drives retrograde F-actin flow in neuronal growth cones. *Neuron.* 16:769–782.

Lockerbie, R., V. Miller, and K. Pfenninger. 1991. Regulated plasmalemmal expansion in nerve growth cones. *J. Cell Biol.* 112:1215–1217.

Lu, M., W. Witke, D. Kwiatkowski, and K. Kosik. 1997. Delayed retraction of filopodia in gelsolin null mice. *J. Cell Biol.* 138:1279–1287.

Martin, M., C. Andreoli, A. Sahuquet, P. Montcourrier, M. Algrain, and P. Mangeat. 1995. Ezrin NH2-terminal domain inhibits the cell extension activity of the COOH-terminal domain. *J. Cell Biol.* 128:1081–1093.

Martin, M., C. Roy, P. Montcourrier, A. Sahuquet, and P. Mangeat. 1997. Three determinant in ezrin are responsible for cell extension activity. *Mol. Biol. Cell.* 8:1543–1557.

Mascotti, F., A. Cáceres, K. Pfenninger, and S. Quiroga. 1997. Expression and distribution of IGF1 receptors containing a β-subunit variant (β-gc) in developing neurons. *J. Neurosci.* 17:1447–1459.

Mitchison, T., and M. Kirschner. 1988. Cytoskeletal dynamics and nerve growth. *Neuron.* 1:761–772.

Morfini, G., S. Quiroga, A. Rosa, K. Kosik, and A. Cáceres. 1997. Suppression of KIF2 in PC12 cells alter the distribution of a growth cone nonsynaptic membrane receptor and inhibits neurite extension. *J. Cell Biol.* 138:657–669.

Nakata, T., and N. Hirokawa. 1987. Cytoskeletal reorganization of human platelets after stimulation revealed by the quick-freeze deep-etch technique. *J. Cell Biol.* 106:1771–1780.

Pfenninger, K., and M. Mayle-Pfenninger. 1981. Lectin-labeling of sprouting neurons. II. Relative movement and appearance of glycoconjugates during plasmalemmal expansion. *J. Cell Biol.* 89:547–559.

Pfenninger, K., L. Ellis, M. Johnson, L. Friedman, and L. Somlo. 1983. Nerve growth cones isolated from fetal rat brain: subcellular fractionation and characterization. *Cell.* 35:573–584.

Pigino, G., G. Paglini, L. Ulloa, J. Avila, and A. Cáceres. 1997. Analysis of the expression, distribution and function of cyclin dependent kinase 5 (cdk5) in developing cerebellar macroneurons. *J. Cell Sci.* 110:257–270.

Quiroga, S., S. Garofalo, and K. Pfenninger. 1995. Insulin-like growth factor I receptors of fetal brain are enriched in nerve growth cones and contain a b-subunit variant. *Proc. Natl. Acad. Sci. USA.* 92:4309–4312.

Roy, C., M. Martin, and P. Mangeat. 1997. A dual involvement of the amino-terminal domain of ezrin in F- and G-actin binding. *J. Biol. Chem.* 272: 20088–20095.

Sato, N., S. Yonemura, T. Obinata, Sa. Tsukita, and Sh. Tsukita. 1991. Radixin, a barbed end-capping actin-modulating protein is concentrated at the cleavage furrow during cytokinesis. *J. Cell Biol.* 113:321–330.

Sato, N., N. Funayam, A. Nagafuchi, S. Yonemura, Sa. Tsukita, and Sh. Tsukita. 1992. A gene family consisting of ezrin, radixin and moesin. Its specific

localization at actin filament/plasma membrane association sites. *J. Cell Sci.* 103:131–143.

Schwartz-Albiez, R., A. Merling, H. Spring, P. Moller, and K. Koretz. 1995. Differential expression of the microspike-associated protein moesin in human tissues. *Eur. J. Cell Biol.* 67:189–198.

Takeuchi, K., N. Sato, H. Kasahara, N. Funayama, A. Nagafuchi, S. Yonemura, Sa. Tsukita, and Sh. Tsukita. 1994. Perturbation of cell adhesion and microvilli formation by antisense oligonucleotides to ERM family members. *J. Cell Biol.* 125:1371–1384.

Tanaka, E., and J. Sabry. 1995. Making the connection: cytoskeletal rearrangements during growth cone guidance. *Cell.* 83:171–176.

Tsukita, Sa., Y. Hieda, and Sh. Tsukita. 1989. A new 82 kD-barbed end capping protein localized in the cell-to-cell adherens junction: purification and characterization. *J. Cell Biol.* 108:2369–2382.

Tsukita, Sa., K. Oishi, N. Sato, J. Sagara, A. Kawai, and Sh. Tsukita. 1994. ERM family members as molecular linkers between the cell surface glycoprotein CD44 and actin-based cytoskeletons. *J. Cell Biol.* 126:391–406.

Tsukita, Sa., S. Yonemura, and Sh. Tsukita. 1997. ERM proteins: head to tail regulation of actin-plasma membrane interactions. *TIBS (Trends Biochem. Sci).* 22:53–58.

Weinhofer, E., L. Zhao, and C. Cohan. 1997. Actin dynamics and organization during growth cone morphogenesis. *Cell Motil. Cytoskelet.* 37:54–71.

Winckler, B., Ch. Gonzalez-Agosti, M. Magendantz, and F. Solomon. 1994. Analysis of a cortical cytoskeleton structure: a role for ezrin-radixin-moesin (ERM proteins) in the marginal band of chicken erythrocytes. *J. Cell Sci.* 107:2523–2534.